JOURNAL OF PROPULSION AND POWER
Vol. 17, No. 5, September–October 2001

Flame-Spreading Phenomena in Fin Slots of a Solid Rocket Motor

K. K. Kuo,* R. A. Kokal,† M. Paulauskas,‡ and P. Alaksin‡
The Pennsylvania State University, University Park, Pennsylvania 16802
and
L. S. Lee§
Lockheed Missiles and Space Company, Inc., Sunnyvale, California 94086-3504

Flame-spreading processes in the fin-slot regions of solid-propellant motor grains have the potential to influence the behavior of the overall ignition transient. The research conducted in this investigation is aimed at obtaining a better understanding of the flame-spreading processes in rocket motors with aft-end fin slots. Nonintrusive optical diagnostic methods were employed to acquire flame-spreading measurements in the fin-slot region of a subscale rocket motor. Highly nonuniform flame-spreading processes were observed in both the deep and shallow fin regions of the test rig. The average flame-spreading rates in the fin-slot region were found to be two orders of magnitude less than those in the circular port region of a typical rocket motor. The flame-spreading interval was found to correlate well with the local pressurization rates. A higher pressurization rate produces a shorter flame-spreading time interval.

Introduction

ALTHOUGH many researchers have studied the flame-spreading processes over simple solid-propellant slabs in laboratory-scale motors and propellant grains with simple geometries in actual rocket motors,[1] little work has been done in the study of flame spreading in rocket motor propellant grains with fin slots. Propellant grains with fin slots have been used in a variety of propulsion systems in both head-end and aft-end applications. In head-end applications the large propellant surface area of the fins is often helpful for achieving a high thrust in a short period of time, as in the case of the space shuttle solid rocket booster.[2,3] For motors with submerged nozzle designs, grain configurations with fin slots in the entrance region to the nozzle allow the high-velocity combustion products to expand into the large free volume, hence reducing the effect of erosive burning.[4] Fin slots can also be used in the aft-end region to increase the total burning surface area. In general, propellant grains with fin slots have several advantages, such as 1) larger burning surface area allowing the overall length of the motor to be reduced; 2) relatively constant total burning surface area of the propellant grain, providing nearly constant thrust level over a major portion of the motor operation period; 3) reduced chance for erosive burning; 4) more propellant surface area for igniter gas to heat the propellant grain for achieving greater reliability; and 5) larger free volume for the pyrogen igniter gases to expand, thereby reducing the localized hoop stress on the motor case.

Depending on the desired thrust characteristics of the motor, the depth of fin slots need not be uniform for all fin slots; a shallow-fin slot and deep-fin slot may alternate around the propellant grain.[5] Figure 1 shows a generic solid-propellant grain with several identical fin slots in propellant grain at the aft end of the motor (finocyl configuration) as reported by Zeller.[5] Some motors have fin slots at the head end regions, as described by Sutton.[6] Because of the complicated geometry of grains with fin slots, the flowfield and flame-spreading process is also intricate and highly three-dimensional. The effects of slot geometry on the flowfield in a solid rocket motor were studied by Waesche et al.[7,8] In view of the complicated geometry and the associated inability to gain sufficient optical access to the propellant grain surface, researchers in the rocket propulsion field have not observed and measured the flame-spreading phenomena in fin-slot regions.

The objective of this work is to obtain better understanding of the flame-spreading event in a solid rocket motor with aft-end fin slots. The specific tasks conducted for achieving the major objective of this study are 1) design a laboratory-scale motor capable of simulating the flame-spreading process in the aft-end fin-slot region; 2) observe and measure the flame-spreading characteristics using nonintrusive optical diagnostic techniques; 3) study the effects of operating conditions, such as chamber pressure, pressurization rate, and igniter strength on the flame-spreading rate; 4) study the relationship between the penetrating gas stream and flame-front propagation directions in fin slots; and 5) develop a flame-spreading correlation useful for design of this type of rocket motors.

Method of Approach

Test Rig Design

To investigate the effects of different parameters on the flame-spreading process in a solid rocket motor with fin slots, the test rig must be sufficiently versatile in design for easy change of test conditions. The test rig must also avoid the use of large amounts of propellant for both safety and economic reasons. The test rig must have an adequate amount of propellant to simulate the flame-spreading process (i.e., thickness of the propellant has to provide a thermally thick environment during the flame-spreading interval). The test rig design must be able to simulate both shallow-fin and deep-fin regions for propellant grains with alternate fin-slot depths. The test rig also has to accommodate the appropriate instrumentation for measurement and observation of the flame-spreading event. The resulting test rig is a subscale analog motor with many suitable features for simulating flame-spreading processes in motors with fin slots.

To view directly the deep-fin and shallow-fin regions, a single triangular fin section of a motor was simulated. The test rig (see Figs. 2 and 3) used in this flame-spreading study consisted of a head-end igniter, a barrel section, a fin-slot section, and a submerged nozzle. Design calculations showed that the motor analog was capable of sustaining high pressurization rates generated by propellant product gases during the ignition-transient interval. The igniter section, which generates hot gases to simulate a pyrogen igniter, could accommodate either one or two cartridge-load igniter grains, which were cast inside phenolic tubes. Most of the tests conducted for this

Received 1 November 1993; revision received 12 October 1996; accepted for publication 17 April 2001.

*Distinguished Professor of Mechanical Engineering and Director of the High Pressure Combustion Laboratory, Mechanical Engineering Department. Fellow AIAA.
†Graduate Student, Mechanical Engineering Department; currently Technical System Engineer, Owens-Corning, Hunting, Pennsylvania.
‡Undergraduate Assistant, Mechanical Engineering Department.
§Research Specialist, Missiles and Space Operators.

study used only one igniter propellant cartridge, in which case a hollow brass spacer was substituted for the other igniter cartridge. Electrical energy was supplied through a remote control system to initiate ignition of the M100 electric match, which then ignited a bag of black powder. Combustion products from the black powder were discharged onto the igniter propellant surface inducing ignition and flame spreading. The pressure-time history of the igniter chamber was recorded by a diaphragm type of pressure gauge (G1). The hot products from the igniter propellant combustion were discharged through a converging–diverging nozzle into the barrel section of the test rig, which simulated the long cylindrical portion of a rocket motor grain. The barrel section propellant grain was also a cartridge-load propellant grain cast in a phenolic tube.

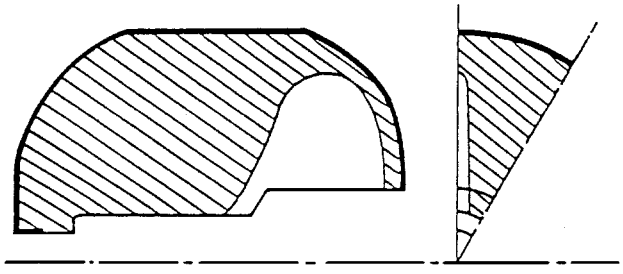

Fig. 1 Generic solid-propellant rocket motor grain with fin-slot design at the aft-end (adapted from Ref. 6).

For each of the tests, a fin-slot sample cast with either live or inert propellant was loaded into the fin-slot section of the test rig. The pressure variations in the fin-slot section were recorded by two pressure transducer gauges (G2 and G3). A submerged nozzle was inserted in the downstream portion of the fin-slot section. Optical access for either the photodetector array or windows for high-speed movie and video cameras was provided on the deep-fin side, and windows were provided on the shallow-fin side of the test rig. To control the chamber pressure and pressurization rates of the test rig, three interchangeable graphite nozzle inserts with diameters of 1.5, 1.75, and 2.0 in. (3.81, 4.44, and 5.08 cm) were used.

Instrumentation

To observe the flame-spreading event and measure the rates and direction of flame-front propagation, the test setup was instrumented with a high-speed HYCAM movie camera, a Spin Physics video camera, and an infrared photodetector array. Based upon a recent study by Thynell et al.[9] using Fourier-transform infrared (FTIR) spectrometry, it was shown that the optical signals from an ignited propellant surface could be distinctly differentiated from those of an unignited propellant surface, even in the presence of combustion product gases and metal-oxide particles in the line-of-sight measurement. The selection of the infrared photodetector array was

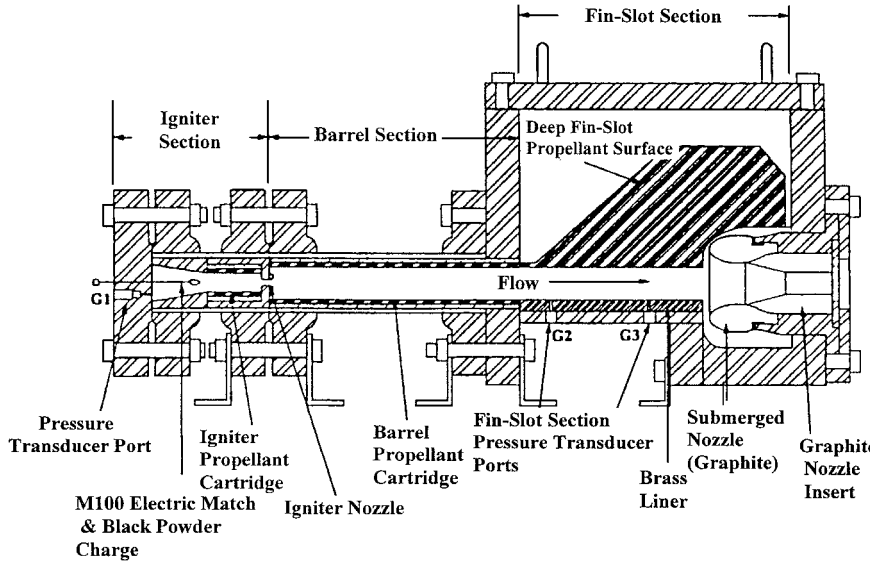

Fig. 2 Cutaway view of flame-spreading test rig and main components.

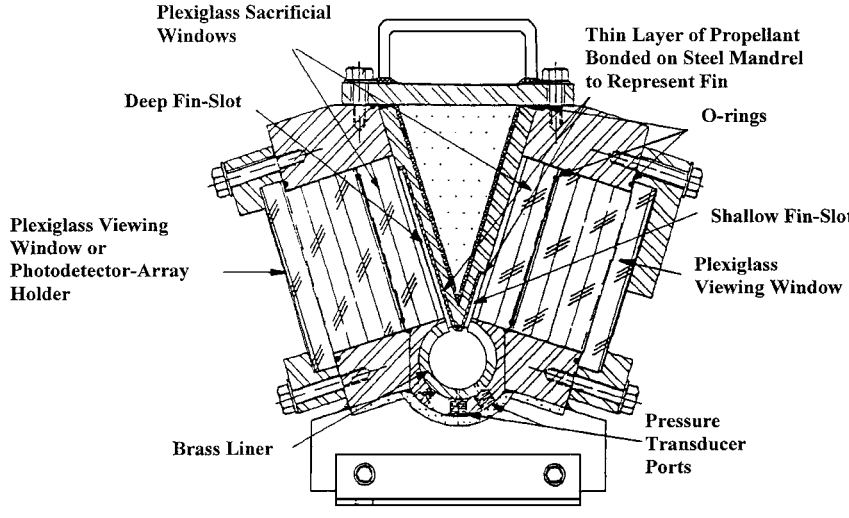

Fig. 3 Cross-sectional view of fin-slot region.

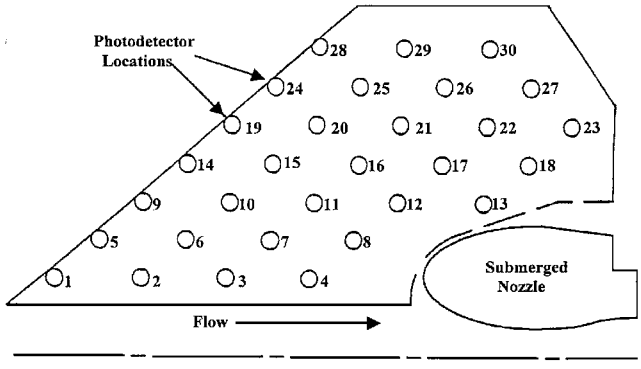

Fig. 4 Photodetector array in the deep fin-slot region.

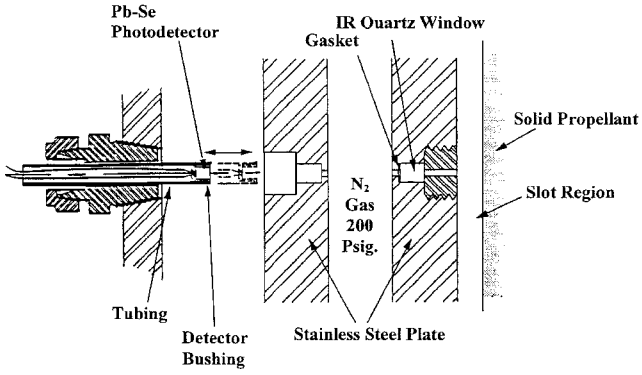

Fig. 5 Cross-sectional view of an optical access port for photodetector measurement.

based upon the three criteria outlined by Thynell et al.[9] for detecting flame-spreading using emitted radiant energy: 1) each measurement location must have an adequate optical access for detection of onset of ignition, 2) emitted energy from the burning surface must be distinguishable from the flowing combustion product gases, and 3) the measurement system must be capable of recording the rapidly changing event. The selected mid-IR photodetector array, consisting of numerous Pb-Se photodetectors, was able to meet all three criteria.

Optical access to the propellant was achieved through a wall of the combustion chamber with 30 small access ports for the photodetectors. The 30 detectors were arranged in an array adequately covering representative regions of the entire propellant surface as shown in Fig. 4. These detectors provided the ignition delay times of 30 different sites of the sample opposite to the photodetectors. A cross-sectional view of one of the optical access ports for photodetector measurement is shown in Fig. 5. A low-pressure nitrogen purge gas between the rigidly mounted stainless-steel plates was used to reduce the force acting on the quartz windows by combustion product gases. The selected IR quartz windows not only effectively shielded the detectors from the hot combustion products, but also transmitted the appropriate infrared emission signals to the photodetectors.

To differentiate the burning propellant surface emitted radiant energy from the flowing combustion product gases emitted radiant energy, a mid-IR wave-number range of 4500 to 2500 cm^{-1} (2.2.–4.0-μm wavelength) range was determined with the FTIR spectrometer. In order to take advantage of the IR emission properties of the propellant ignition and to meet the criteria of fast-response, lead-selenide photodetectors (<10-μs temporal response; 1–4.5-μm wavelength) with optical filters were selected. The filters eliminated detection of wavelengths beyond the 4.0-μm range, thus effectively eliminating the detection of a significant combustion product emission. Several tests were conducted to ensure that the detectors did not respond significantly to upstream combustion product gases and metal-oxide particulates. The detectors showed only a slight response to igniter propellant product gases, but when exposed to propellant ignition they had a significant response indicated by a sharp peak, proving their capability for distinguishing the ignition event from combustion product gases. The photodetector data were acquired using a PC-based data-acquisition system, which obtained data at a rate of 1000 samples per second. Theoretically, one should use a much higher speed data-acquisition system for these measurements, but the relatively slow flame-spreading rates discussed in the Results and Discussion section justify the use of PC-based data-acquisition system. With the preceding data-acquisition system the time variation of intensity of the IR emission from the propellant showed sufficiently rapid rise at ignition. Therefore, the ignition-delay time at specific locations could be accurately determined from the intensity vs time plots recorded by the array of detectors.

The high-speed movie films of the deep and shallow fin-slot regions also provided a detailed view of the flame-spreading phenomenon. Large Plexiglas® windows provided optical access to nearly the entire deep-fin and shallow-fin propellant surfaces. For most tests the camera obtained images at a rate of 6000 pictures per second, this is sufficiently fast for capturing the flame-spreading event.

Two different flow-visualization techniques (surface flow visualization and flow direction tracer) were used to determine the general flow pattern in the fin-slot region under cold and noncombusting flow conditions. The surface flow visualization was accomplished using a chalk and kerosene mixture painted on the inner surface of the Plexiglas window surface. For the flow direction tracer method small threads were taped to many locations along the window surface, and a video camera recorded the flow pattern indicated by the tracers.

Results and Discussion

The overall ignition transient based upon the recorded pressure-time traces during this study showed many similarities to the ignition-transient process for a typical solid rocket motor described by Kumar and Kuo.[1] The pressure-time traces for a typical test recorded at the three pressure gauge locations are shown in Fig. 6.

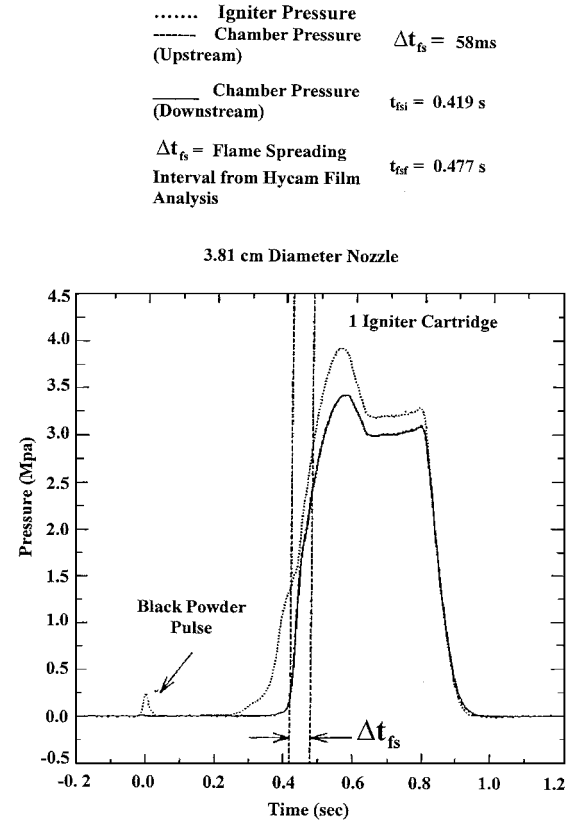

Fig. 6 Typical set of pressure-time traces for a flame-spreading test in a motor with fin slots.

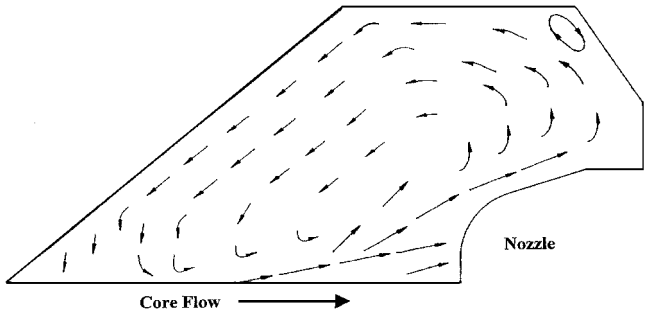

Fig. 7 Flow pattern in the deep fin-slot region obtained from a cold-flow test.

The igniter chamber pressure, recorded by Gl, initially showed a small pressure pulse caused by the ignition of the black powder charge. The easily distinguishable peak of the black powder pulse was defined as time zero for all other instrumented channels. Following ignition and flame spreading along the igniter propellant grain, the igniter chamber pressure rose as a result of the choking of the upstream nozzle by the product gases leaving the igniter section. Pressure transducers G2 and G3 recorded nearly identical responses for the test duration, showing evidence of little or no axial variation in pressure at the opening of the fin-slot region. All pressures initially overshot about 10% beyond the steady-state operating levels. After a period of steady pressure condition, all gauges indicated a rapid drop to atmospheric pressure as the propellant grain burned out. The two vertical dashed lines in Fig. 6 represent the flame-spreading interval determined from time-correlated information from the high-speed movie films. The flame-spreading interval was also determined from the photodetector signals when the detector array was used instead of the movie camera. The pressure-time traces were varied by changing the throat area of the exit nozzle and/or the number of igniter propellant grains. Tests conducted under the same conditions were found to be highly reproducible. Recorded pressure-time traces for all test firings indicated expected changes with respect to the test setup and operating conditions.

The resulting flow patterns obtained by the flow-visualization studies showed very interesting behavior in both the shallow-fin and deep-fin regions. Figure 7 shows the flow pattern in the deep fin-slot region obtained under cold flow conditions, using the aforementioned flow-visualization techniques. In this figure longer arrows were used to represent the flow in higher velocity regions and shorter arrows for flows in lower velocity regions. It was found that the inertia of the core flow in the fin-slot section along the motor axial direction has a strong influence on the resulting flow pattern in the fin slot. A stronger core flow usually results in a smaller angle of penetration into the fin-slot region immediately in front of the submerged nozzle. A portion of the core flow was found to deflect into the top portion of the fin-slot region above the submerged nozzle. Because of the geometric shape of the local free volume, the flow first turned counterclockwise, then turned downward along the inclined edge of the sample, and then entrained a portion of the core flow to enter into the large recirculating flow region in the center portion of the deep fin-slot region. A small clockwise counter-rotating flow was evident in the upper right corner of the fin-slot region. Flame-spreading patterns for the low-pressure test runs using a larger 2.0-in. (5.08 cm)-diam nozzle provided evidence that another small counter-rotating flow may have existed in the upper left corner near the inclined edge. Although the flow patterns obtained under cold flow conditions were only valid when gas generation was negligible in the fin-slot region, the flow pattern seemed to have a strong influence on the flame-spreading phenomena. It is interesting to mention that, as observed in the flow-visualization work of Waesche et al.[7] on the aft-end internal flowfields of candidate space shuttle boosters and a high-performance motor, the flow pattern in the fin-slot region depends strongly upon the motor configuration and the flow conditions in the core region. The recirculating flow in the fin-slot region induced by the core flow also depends strongly on the flow conditions in the core region. Therefore, it is expected

Region	Time (ms)	Region	Time (ms)
1	419	8	463
2	426	9	467
3	428	10	470
4	432	11	473
5	436	12	475
6	442	13	477
7	454		

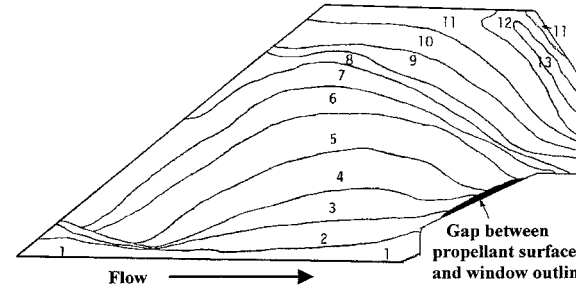

Fig. 8 Flame-front contours in the deep fin-slot region.

that the core flow conditions should have a profound influence on the flame-spreading phenomena in the fin-slot region.

The flame-front propagation contours at different times were obtained from the image analysis of the high-speed movie films. To obtain the contours, the films were viewed frame by frame against a paper screen. A pulsed light emitting diode (LED) system provided selected timing pulses of light to which the edge of the film was exposed. This allowed the flame contour from the film to be outlined on the paper at specific times. A 2-ms common-time signal was also generated from the high-speed movie camera system during the remote triggering of the ignition event so that both the film and the pressure data were correlated. The flame-front contours shown in Fig. 8 correspond to the pressure-time traces shown in Fig. 6. In Fig. 8 the bottom region (region 1) ignited first because of the strong core flow, as it flowed over the slightly protruded fin tip into the circular port shown in Fig. 3. Because the primary mode of heat transfer in a major portion of the fin-slot region is forced convection (as justified by heat transfer calculations), successive ignition was expected, and the flame front propagated into the center portion of the fin-slot region with gradual changes in flame-front curvatures.

The flame front initially spread slowly in the upstream portion of the fin-slot region near the bottom of the propellant sample and then spread more quickly along the inclined edge. Part of the reason for the initial delay in the upstream region can be attributed to the high inertia of the core flow, which did not give the flow a chance to expand into the fin-slot region until it approached the submerged nozzle (see Fig. 7). In fact, the flow direction in this region was primarily in the downstream direction along the motor axis. Thus, the propellant in the inclined region of the fin slot was not initially exposed to high heating rates. The flow pattern in Fig. 7 provides some evidence of the weak flow in the upstream region induced by recirculating gases in the fin-slot region. The flame-front curvature increased as it passed the center of the recirculating flowfield. After region 7 of Fig. 8, the flame front propagated rapidly along the inclined surface. This was largely because of the increased propellant burning surface area per unit free volume along the inclined edge where the side propellant surface intersected with the main propellant surfaces in the fin-slot region.

The flame-front propagation into the upper right corner of the fin slot above the submerged nozzle also showed a significantly delayed ignition. The delayed flame spreading to this region is believed to be caused by the entrainment of cool air in the recirculating zone, which was evident in the flow pattern of the deep fin. It is useful to point out that the radiative heat-transfer mode was not important, otherwise this edge region, which has a much better view factor than the major portion of the propellant surface in the fin slot, would ignite first. Most of the flame-spreading patterns showed evidence of delayed ignition in this corner region. The low-pressure test case also showed delayed ignition in the opposite corner indicating the

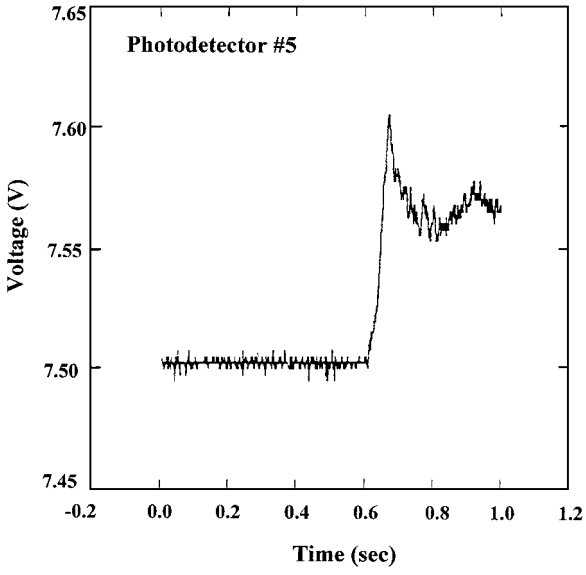

Fig. 9 Typical photodetector response.

presence of another recirculating zone in that location. Although the flame-front propagation patterns showed some similarities under different operating conditions, the flame-front propagation rate was found to be a function of the operating conditions. For example, the recirculating zone in the corner near the inclined edge was only evident in the lowest pressure condition tested. In addition, for the test run with two igniter grains a large amount of turbulence was evident in the upstream region near the entrance to the fin-slot region.

The responses of the photodetectors also provided very useful information about the flame-spreading process in the deep fin-slot region. A typical photodetector response is shown in Fig. 9. The sharp rise in the signal corresponds to the onset of ignition of the propellant surface located opposite to the photodetector port. The ignition-delay time at each location was determined by intersecting the slope of the sharp rise of the intensity-vs-time plot with the time axis. In nearly all tests using the photodetector system, detector #4 near the nozzle (see Fig. 4) was the first one to respond, confirming the results obtained in the film analysis. Other interesting results obtained by the detectors were the early response of a few detectors along the lower edge of the inclined surface and the delayed response of detector #23. As was mentioned earlier in the discussion of the film analysis, the flame may spread more quickly along the inclined surface because of larger specific burning surface area. The delayed response of detector #23 was essentially caused by the recirculating flow near the upper right corner. Because of the ability of the IR detectors to distinguish between unburned and burned surfaces even with flowing combustion products as the media between the photodetector and the sample surface, the photodetectors provided reliable data for determining ignition-delay times at specific locations. The flame-front contours obtained from the movie film analysis provided more general information about flame-spreading phenomena and made it possible to observe the changes in flame-spreading patterns under various operating conditions. Again, the flame-spreading contour would be very different if radiative heat transfer were important; the edge zone along the whole fin slot would be the first place to ignite.

For the shallow fin-slot region a typical flow pattern is shown in Fig. 10, and the flame-spreading pattern determined from the film analysis is shown in Fig. 11. A comparison of these two figures indicated that the flame-spreading pattern was closely related to the flow pattern of the cold flow. The flow pattern was a function of the chamber operating condition. A test conducted under a relatively low-pressure condition indicated less core gas penetration into the corner above the submerged nozzle and also showed the presence of an upstream recirculating zone. The reasons for ignition delay in the recirculating regions are similar to those discussed for the deep fin.

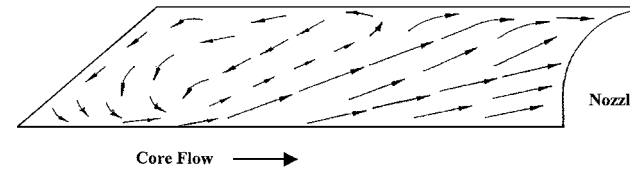

Fig. 10 Flow patterns in the shallow fin-slot region.

Using the results of the film analysis, average flame-spreading velocities were deduced for both the deep and shallow fins. An average flame-spreading velocity was defined as the time derivative of the ignited area of the fin bounded by the flame front divided by the average length of the flame front, namely,

$$V_{\mathrm{fs}}(t) = \frac{1}{L_{\mathrm{ff}}(t)} \frac{\mathrm{d}A_{\mathrm{ignited}}}{\mathrm{d}t} \tag{1}$$

To obtain the time derivative of the burning surface area, the instantaneous surface area was determined through image analysis on a Macintosh-based image processor. The time variation of the area was fitted with a fourth-order polynomial and then differentiated. The expression for the derivative was then divided by a fourth-order fit of the average length of the instantaneous flame front. The average flame-spreading velocity variations in the deep fin-slot region for four different operating conditions are shown in Fig. 12. The results were plotted on the same vertical and horizontal scale for convenience of comparison. The time variations of the burning surface area and average flame-spreading rate show similar trends among these four tests.

The effect of exit nozzle diameter can be seen from the comparison of test conditions a), b), and d). For a larger exit nozzle the chamber pressure and pressurization rate were lower; hence, the flame-spreading interval was longer. The initial decay of flame-propagation speed in these three cases can be attributed to the delay of flame-spreading processes by the recirculating flow behavior inside the fin-slot region. The relatively cold gases in the recirculating zones inhibited penetrative motion by the core gas composed of hot propellant products. After reaching a minimum, the flame-propagation rate increased quickly as a result of the fast flame-spreading rate along the edge (fin-slot tip) region where the specific burning surface area was high. In addition, as the fin slot was filled with more propellant product gases from the ignited surfaces the heat-transfer rate increased, thereby facilitating faster flame spreading. Further generation of combustion products then drove the flame front into the small remaining free volume of the fin slot above the submerged nozzle until the flame completely engulfed the fin-slot sample. Comparing cases a), c), and d), it is observed that the higher the pressurization rate (corresponding to the smallest exit nozzle diameter), the shorter the overall flame-spreading interval and the higher the maximum flame-spreading rate.

By comparing the test results in b) and c) of Fig. 12, the effect of the igniter strength on flame spreading is quite obvious. Stronger igniters [case c)] produce higher flame-spreading rates and shorter flame-spreading time intervals.

Another interesting flame-spreading phenomena exhibited in Fig. 12 is the relatively low flame-spreading rate in comparison with those observed in the circular bore region. The typical flame-spreading rates in a circular bore after an initial acceleration can reach speeds up to several hundred meters per second. In view of this fact and the slow flame-spreading rate in the fin-slot region, it is easily conceivable that the overall ignition transient processes in a solid rocket motor with fin slots is rate limited by the relatively slow flame-spreading phenomena in the fin-slot region.

In the development of an empirical correlation for flame-spreading interval, it is useful to consider the effect of pressure, pressurization rate, and igniter strength on the flame-spreading rate in the fin-slot region. To quantify the effect of motor operating conditions over the flame-spreading time interval, the following correlation was developed based upon the data obtained from this study:

$$\Delta\tau_{\mathrm{fs}} = \frac{C}{(\mathrm{d}P^*/\mathrm{d}t^*)^{n_1}(P^*)^{n_2}} \tag{2}$$

Region	Time (ms)	Region	Time (ms)
1	402	6	418
2	409	7	420
3	413	8	423
4	415	9	428
5	416		

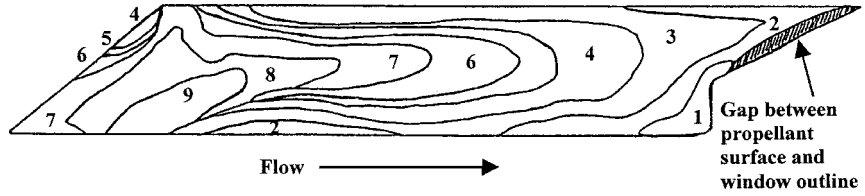

Fig. 11 Flame-front contours in the shallow fin-slot region.

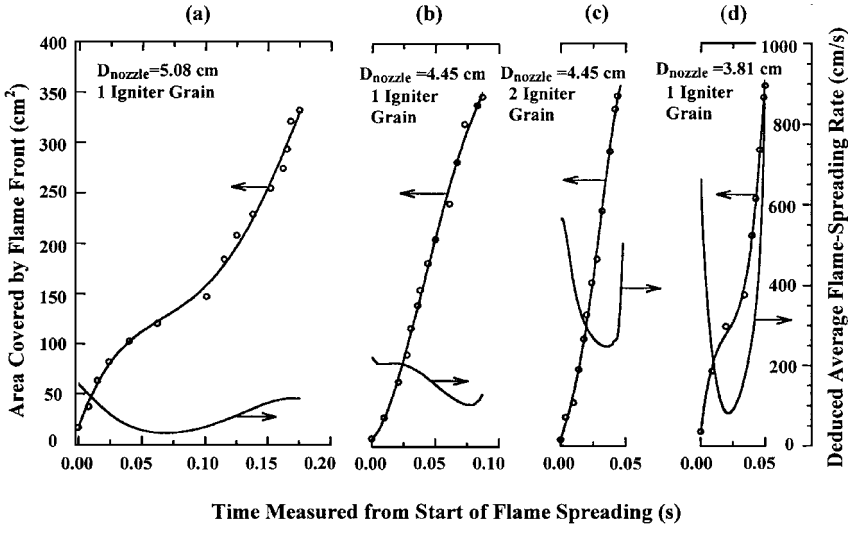

Fig. 12 Deduced flame-spreading rates in fin-slot region for four representative tests.

where dP^*/dt^* is the dimensionless pressurization rate during flame spreading and P^* is the dimensionless pressure defined as the average pressure during flame spreading, divided by a reference pressure of 1 atm.

$$P^* \equiv (P_1 + P_2)/2P_{\text{atm}} \tag{3}$$

where P_1 and P_2 are the average chamber pressure at the corresponding times t_1 and t_2, representing the beginning and ending of the flame-spreading interval.

The dimensionless flame spreading time interval $\Delta\tau_{\text{fs}}$ is defined as

$$\Delta\tau_{\text{fs}} \equiv (t_2 - t_1)/t_{\text{res}} \tag{4}$$

where t_{res} is the flow residence time over the axial length of the fin-slot region. The residence time of the core flow through the fin-slot section can be defined as

$$t_{\text{res}} \equiv L_{\text{fin-slot}}/V_{\text{bore}} \tag{5}$$

where V_{bore} is the bulk velocity of the core gas at the axial station immediately upstream of the fin-slot region. The test data were analyzed using the proposed functional form based upon Eq. (2) and a standard multiregression analysis. The correlation obtained has the following form:

$$\Delta\tau_{\text{fs}} = \frac{22.95}{(dP^*/dt^*)^{0.6689}} \tag{6}$$

The pressure, P^* has been found to have very little influence on the dimensionless flame-spreading interval $\Delta\tau_{\text{fs}}$. The value of exponent n_2 was found to be much smaller than the value of n_1; therefore, the influence of average pressure on the flame-spreading rate can be eliminated. Based upon the data analysis and the correlation, the pressurization rate was found to be the governing parameter controlling the overall flame-spreading interval. From a physical point of view, the inherently transient phenomena of flame spreading into the fin-slot region are governed by the gas penetration and the recirculating flow processes in the localized region. The higher the localized pressurization rate, the stronger the product gas interactions with the unburned propellant causing higher heat feedback to the unburned surface; therefore, the overall flame-spreading interval is shorter. Figure 13 shows the comparison of the experimentally determined flame-spreading interval with the correlated flame-spreading interval. The experimental results, using the diagnostic techniques already mentioned, are in very close agreement with the correlation; nearly all of the data fall within 15% of the correlated results.

Based upon the preceding fin-slot flame-spreading correlation, the pressurization rate in the entrance to the fin-slot region exhibited a dominant influence on the overall flame-spreading interval. In practice, higher pressurization rates can be generated using a smaller diameter exit nozzle or by increasing the igniter mass flow rates. Both of these methods resulted in shorter flame-spreading intervals. Because the correlation is given in dimensionless form, it is believed that this kind of correlation can be used as a design tool by motor designers. However, caution must be exercised in the usage of the preceding correlation, especially when the grain geometry is very different from the one considered in this study.

Summary and Conclusions

1) A subscale motor was successfully designed and fabricated for the study of flame spreading and flow phenomena in the fin-slot region containing both deep and shallow fins.

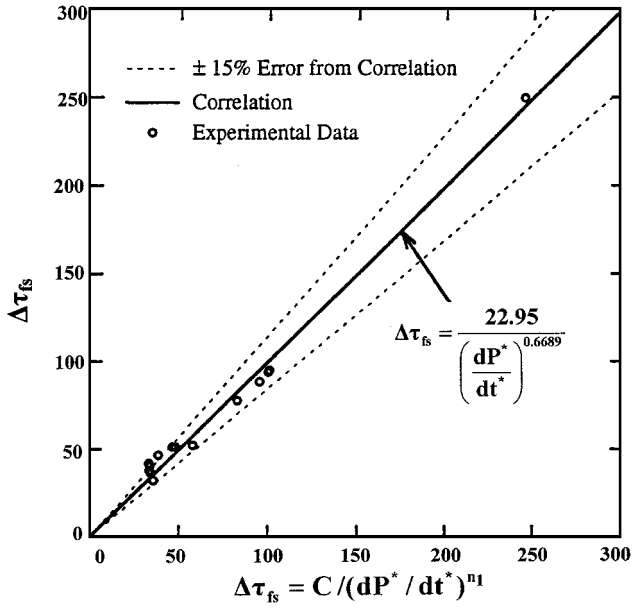

Fig. 13 Comparison of flame-spreading correlation with experimental data.

2) A new photodetector system together with high-speed movie cameras were employed for detecting the onset of ignition at a localized region and studying flame-spreading phenomena.

3) Test results showed the following interesting behavior:

a) Highly nonuniform flame-spreading processes occurred in both the deep and shallow fin regions.

b) The flow pattern in the fin-slot region exhibited a strong coupling with the flame-spreading pattern. The recirculating flows near the corner regions of the fin slot generally retarded the flame-spreading process.

c) Observed flame-spreading rates in the fin-slot regions were significantly lower than those of a typical circular bore region. This shows the rate-controlling characteristics of the flame- spreading process in the fin-slot regions in the overall ignition and thrust transients of solid rocket motors with fin slots.

d) The level of average flame-spreading rate V_{fs} and the flame-spreading interval $\Delta\tau_{fs}$ were found to depend strongly upon the pressurization rate at the opening of the fin-slot region.

4) A dimensionless correlation was developed based upon test data. The dependency of the overall flame-spreading interval on the local pressurization rate was determined. The higher the pressurization rate, the stronger the product gas interaction with the unburned propellant surface, and therefore, the shorter the flame-spreading interval. This correlation, given in dimensionless parameters, could be useful to motor designers. Deeper understanding of the complicated flame-spreading process in a three-dimensional motor grain was also achieved by this investigation.

Acknowledgments

The authors would like to acknowledge the support and encouragement of Lockheed Missiles and Space Company, Inc., (LMSC) for this challenging research conducted at the High Pressure Combustion Laboratory of The Pennsylvania State University (PSU). The encouragement of Frank Bogart and Walt E. Moffat of LMSC is deeply appreciated. We would also like to thank the Thiokol engineers, including Randy Jardine and Darrall Reese, for their collaboration in propellant sample casting and shipment.

The authors are indebted to Taras Jarymowycz and Randy Salizzoni of PSU for their active participation and contribution during the early phase of this project.

References

[1]Kumar, M., and Kuo, K. K., "Flame Spreading and Overall Ignition Transient," *Fundamentals of Solid Propellant Combustion*, edited by K. K. Kuo and M. Summerfield, Vol. 90, Progress in Astronautics and Aeronautics, AIAA, New York, 1984, pp. 305–360.

[2]Timnat, Y. M., *Advanced Chemical Rocket Propulsion*, Academic Press, New York, 1987, pp. 197–214.

[3]Gatland, K., *Space Technology*, Salamander Books, Ltd., New York, 1981, pp. 198–213.

[4]Razdan, M. K., and Kuo, K. K., "Erosive Burning of Solid Propellants," *Fundamentals of Solid Propellant Combustion*, edited by K. K. Kuo and M. Summerfield, Vol. 90, Progress in Astronautics and Aeronautics, AIAA, New York, 1984, pp. 515–598.

[5]Zeller, B., "Solid Propellant Grain Design," *Solid Rocket Propulsion Technology*, edited by A. Davenas, Pergamon Press, Oxford, England, U.K., 1993, pp. 35–84.

[6]Sutton, G. P, " Solid Propellant Rocket Fundamentals," *Rocket Propulsion Elements: An Introduction to the Engineering of Rockets*, 6th ed., Wiley, New York, 1992, pp. 365–415.

[7]Waesche, R. H. W., Marchman, J. F., and Kuppa, S., "Effects of Grain and Aft-Dome Configuration on Aft-End SRB Internal Flows," *Journal of Propulsion and Power*, Vol. 7, No. 2, 1991, pp. 163–170.

[8]Waesche, R. H. W., Marchman, J. F., and Kuppa, S., "Effects of Grain Slots on Flow in a Solid Rocket Motor," *Journal of Propulsion and Power*, Vol. 7, No. 2, 1991, pp. 171–177.

[9]Thynell, S. T., Huang, I. T., Kuo, C. S., Hsieh, W. H., and Kuo, K. K., "Approach to Measurements of Flame Spreading over Solid Propellants," *Journal of Propulsion and Power*, Vol. 8, No. 4, 1992, pp. 914–917.